Polarized Supercontinuum Generation in CS_2-Core All-Normal Dispersion Photonic Crystal Fiber

Chao Wang, Kai Lin, Suqun Cao, Guoying Feng, Jun Wang, and Ahmed N. Abdalla

***Abstract*—We numerically analyze a polarization maintaining (PM) supercontinuum generation (SCG) in all-normal dispersion liquid (CS_2)-core photonic crystal fiber (LC-PCF). The proposed LC-PCF affords a high birefringence (10^{-3} to 10^{-2}) from 1.0 μm to 2.2 μm wavelength with fundamental mode behavior. The linear polarization and high coherence spectral width for X and Y polarized axes covers 1.32 μm$\sim$2.28 and 1.28 μm$\sim$2.24 μm with pump wavelength of 1.55 μm at pump power of 2 kW, respectively. Furthermore, we found that the ability of maintaining linear polarization state of SC source for X-axes is better than that of Y-axes as the pulse duration varies from 0.05 ps to 0.6 ps at the same pump wavelength. In addition, the proposed LC-PCF-based SC source is a good candidate for applications such as biomedical imaging, fluorescence lifetime imaging fields, and frequency comb sources.**

***Index Terms*—Liquid core photonic optical fiber, linear polarization state, coherence, supercontinuum generation.**

I. Introduction

SUPERCONTINUUM generation (SCG) in photonic crystal fibers (PCFs) has been studied broadly and deeply more than two decades [1]. They have extensive applications such as in optical communications [1], [2], [3], [4], wavelength-tunable light sources [5], [6], optical frequency metrology [7], [8], [9] and optical coherence tomography (OCT) [10], [11] etc.; However, many applications require linearly-polarized (LP) supercontinuum generation (SC). For instance, linearly-polarized SC for the UV to near-IR region is important in biomedical imaging and fluorescence lifetime imaging fields [12], [13], [14], the hyperspectral imaging system require the SC source to have linear polarization state [15], [16]. The SC applied to ultra-short pulse amplifiers and frequency comb sources in 2 μm spectral region require the source to have linear polarization state [17], [18]. Moreover, it is important to use polarization-maintaining fibers to have a well-defined polarization and phase of seed pulse [16]. In the circularly symmetric fiber, the generated SC is generally unpolarized. The effective way for obtaining a linearly polarized SC is using highly birefringent PCFs [19], [20], [21], [22].

Recently, many researchers have carried out research work to obtain high birefringence, high nonlinearity and dispersion management photonic crystal fibers [23], [24], [25], [26], [27], [28]. The common methods which can achieve high birefringence ($B = 10^{-3}\sim10^{-2}$) are using elliptical or rhombic holes around core or elliptical core [24], [27]. But the incorporation of elliptical air holes or rectangular air holes in or around the core of the structures make fabrication difficult. So the air hole rings of different size arranged in a hexagonal lattice are widely used [23], [26].

The innovative potential of liquid-core photonic crystal fiber (LC-PCF) combines good transmission from visible to middle infrared region (NIR) [29], [30], [31], [32], [33] spectrum with nonlinearities as high as those of soft-glasses, and tuning capabilities comparable to those of gases. A variety of liquid filled optical fibers are used to generate supercontinuum, the liquid including carbon disulfide (CS_2), ethanol (C_2H_5OH), carbon tetrachloride (CCl_4), nitrobenzene ($C_6H_5N_2O$) and water (H_2O) etc. Among these liquids, CS_2 feature highly non-instantaneous nonlinearities [32] and a broad transmission range [34], [35]. D. Churin et al. have demonstrated that the liquid CS_2 has nearly 100% transmission in the wavelength range of 1.4 μm $\sim$2.2 μm by experiment [35]. And CS_2-core optical fiber possesses nonlinear response with picosecond long decay times, which is unique. Such highly non-instantaneous response originates from the strong reorientation and libration of elongated carbon disulfide liquid molecules in an optical field. The resulting nonlinear refractive index ($n_2 \leq 285\times10^{-16}$ $cm^2\cdot W^{-1}$) can be comparable to the soft-glass systems. The process of spectral broadening depends strongly on the fiber dispersion and its nonlinear gain, but also on the temporal characteristics of the core material. So we choose carbon disulfide as the filling liquid. All-normal dispersion (ANDi) supercontinuum exhibits a much superior noise performance [18], [20], [36], [37]. All-normal dispersion optical fibers can be used to efficiently suppress the polarization modulation instability (PMI), and eliminate the last remaining noise amplification process in femtosecond pump ANDi SC

Manuscript received 11 November 2022; accepted 15 November 2022. Date of publication 21 November 2022; date of current version 6 December 2022. This work was supported by the Cooperative Project of production, teaching and researching in JiangSu Province under Grant BY2022213. *(Corresponding authors: Chao Wang; Kai Lin.)*

Chao Wang is with the Huaiyin Institute of Technology, Huaian 223003, Jiangsu, China, also with the Institute of laser and Micro/Nano Engineering, College of Electronics and Information Engineering, Sichuan University, Chengdu 610064, China, and also with the Suzhou Everbright Photonics Co., Ltd, Suzhou Sicence and Technology Town, Suzhou 215163, China (e-mail: chaowang_2005@126.com).

Kai Lin, Suqun Cao, and Ahmed N. Abdalla are with the Huaiyin Institute of Technology, Huaian 223003, Jiangsu, China (e-mail: linkai03@mail.ustc.edu.cn; 501419311@qq.com; dramaidecn@gmail.com).

Guoying Feng is with the Institute of laser and Micro/Nano Engineering, College of Electronics and Information Engineering, Sichuan University, Chengdu 610064, China (e-mail: 1419901623@qq.com).

Jun Wang is with the Institute of laser and Micro/Nano Engineering, College of Electronics and Information Engineering, Sichuan University, Chengdu 610064, China, and also with the Suzhou Everbright Photonics Co., Ltd, Suzhou Sicence and Technology Town, Suzhou 215163, China (e-mail: wjdz@scu.edu.cn).

Digital Object Identifier 10.1109/JPHOT.2022.3223534

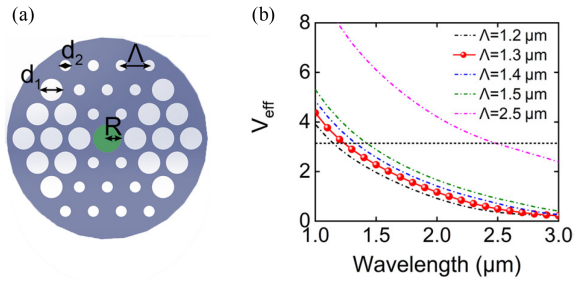

Fig. 1 The crystal geometry structure with a carbon disulfide core (a). V number as a function of wavelengths at $d_1/\Lambda = 0.9$, $d_2/\Lambda = 0.4$. The horizontal dotted line represents $V = \pi$ (b). Fig. 1 was calculated by using Ref [42].

generation [18]. To obtain broadband supercontinuum, the pump wavelength should be selected at or close to the maximum of the convex dispersion curve in all normal dispersion region [38]. Additionally, the wideband spectrum can be generated by appropriately increasing the pulse duration or pump power. Nevertheless, the coherence and polarization of the supercontinuum will deteriorate for large the pulse width and pump power. Xu et al. designed a highly nonlinear polarization-maintain PCF by using two liquids of CS_2 and C_2H_5OH [39]. However there is no report on the nonlinear optical dynamics and SC generation in all-normal dispersion CS_2-core polarization maintaining (PM) PCF with high birefringence. We proposed the PM PCF filled with only one liquid of CS_2. Such PM LC-PCF can pave the way for novel spectroscopic applications and coherent and tunable mid-infrared linear polarization light sources.

This manuscript introduces a highly nonlinear polarization-maintaining (PM) PCF of core-filled with only one liquid (CS_2) in the background of silica and working in all-normal dispersion region (the two polarization principal axes). The proposed LC-PCF has a ultra-high birefringence (in the order of $10^{-3}\sim10^{-2}$) for 1.0$\sim$2.2 μm wavelength. Besides, the two-axes polarization modes exhibit different time sensitivity, which can be interestingly used to guide the actual experiment. Moreover, to validate the polarization spectrum principle of evolution under different pulse duration, and analyze the influence of noise caused fluctuation on polarization state. Numerical simulation of the SCG for a low pump peak power of 2 kW at a pump wavelength of 1.55 μm shows that a broadband polarized continuum from 1.32 μm to 2.28 μm and from 1.28 μm to 2.24 μm for X and Y polarized axes, respectively.

II. Design of LC-PCF and Theoretical Model

A. High Birefringence LC-PCF Numerical Model

Photonic crystal fiber with a core infiltrated with carbon disulfide (CS_2) is proposed as shown in Fig 1(a). The microstructure cladding is composed of three rings of circular air holes, which form a hexagonal lattice in silica glass background. In order to enhance the effective index difference between the two orthogonal polarization modes, we introduce large circular air holes into the cladding. The optical fiber parameters: d_1, d_2, $2R(2R = \Lambda)$ and Λ denote the diameters of large air holes, small air holes, core hole and air hole pitch, respectively. The big hole air-filling fraction of d_1/Λ can be selected in the region of [0.8, 0.9] for high mode birefringence [28], [40], [41]. As triangular lattice PCF exhibits the property that extends the d_2/Λ ratio up to 0.475 while maintaining the single mode characteristics [42]. This feature of the PCF provides a degree of freedom to increase the small air-filling ratio from 0.4 to 0.475. We choose maximum (minimum) value of the big (small)-hole air-filling fraction as $d_1/\Lambda = 0.9$ ($d_2/\Lambda = 0.4$) because the increased (decreased) d_1/Λ (d_2/Λ) will increase the fabrication difficulty. Fig. 1(b) illustrates the changes in V numbers [42] as a function of wavelengths for the proposed PM LC-PCF. It is seen that the V number of the proposed LC-PCF increases as the air hole pitch increases from 1.2 μm to 2.5 μm. The cutoff wavelengths of single mode are 1.15 μm, 1.24 μm,1.33 μm,1.42 μm, 2.50 μm when the air hole pitches are Λ = 1.2 μm, 1.3 μm, 1.4 μm, 1.5 μm, 2.5 μm, respectively.

The refractive index of pure silica and carbon disulfide (CS_2) as a function of wavelength using the following SellMeier equation (at 20 °C):

$$n_{CS_2}^2 - 1 = \frac{1.499426\lambda^2}{\lambda^2 - (0.178763\ \mu m)^2} + \frac{0.089531\lambda^2}{\lambda^2 - (6.591946\ \mu m)^2} \tag{1}$$

where λ is the free space wavelength in units of μm [32]. Carbon disulfide exhibits almost no absorption in the visible and near infrared region [34], [35], [43]. And the definition of group-velocity dispersion (GVD) can be described as:

$$D(\lambda) = -\frac{\lambda}{c}\frac{d^2\mathrm{Re}[n_{eff}(\lambda)]}{d\lambda^2} = -\frac{2\pi c}{\lambda^2}\beta_2 \tag{2}$$

where c, β_2 and $n_{eff}(\lambda)$ are the velocity in free space, the second-order dispersion, and the LC-PCFs effective index of the fundamental mode respectively. We calculated the effective refractive index n_{eff} and the confinement loss (CL) [23] of the fiber by using COMSOL software. Then the birefringence (B), the two polarization modes effective mode area (A_{eff}) and the nonlinear coefficient (γ), the chromatic dispersion (D) and the higher-order dispersion coefficient β_m (m$\geq$2) are calculated [44], respectively. We can control the characteristics of the proposed fiber by adjusting the fiber geometry parameters.

To maintain the single mode characteristics and high birefringence of the proposed fiber, we vary the hole pitch from 1.2 μm to 1.6 μm and fix $d_1/\Lambda = 0.8$ and $d_2/\Lambda = 0.4$. It can be seen from Fig. 2(a), the mode birefringence increases as the hole pitch decreases, the main reason is that the small pitch increases the asymmetry in the structure. It also can be seen from Fig. 2(a) that the birefringence increases as the wavelength varies from 1 μm to 2.2 μm, this is because the smaller pitch increases the asymmetry in structure. Fig. 2(b) shows that the decrease in the hole pitch results in an increase of confinement loss of the two polarized mode. Furthermore, the loss of the fast (Y) axis is greater than that of the slow (X) axis. This is because the mode confined in the core extends into the cladding as the hole pitch decreases, which leads to an increase in loss. Fig. 2(c) shows the dispersion of the designed LC-PCF, the wavelength corresponding to the maximum point of dispersion decreases as the lattice pitch decreases. The results show that the fiber

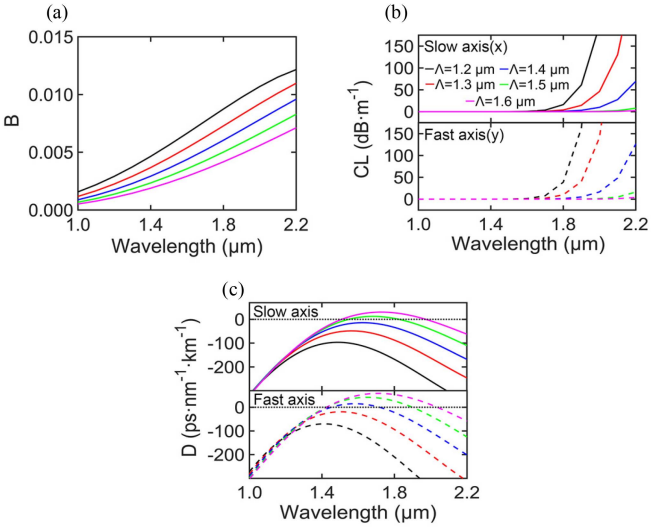

Fig. 2. Variation of wavelength with birefringence (a), confinement loss (b), and GVD parameter D (c) for $\Lambda = 1.2$ μm (black), 1.3 μm (red), 1.4 μm (blue), 1.5 μm (green), 1.6 μm (magenta) at $d_1/\Lambda = 0.8$, $d_2/\Lambda = 0.4$. Fig. 2 was calculated by using Ref [41].

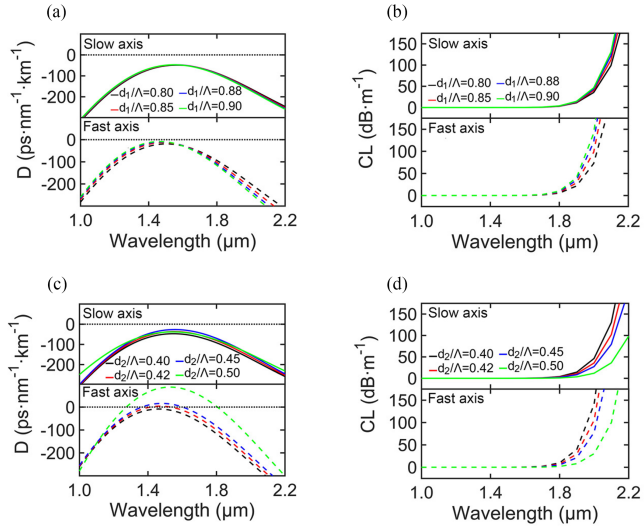

Fig. 3. Group-velocity dispersion D (a) and confinement loss (b) with different d_1/Λ at $d_2/\Lambda = 0.40$, and $\Lambda = 1.3$ μm. GVD parameter D (c) and confinement loss (d) with different d_2/Λ at $d_1/\Lambda = 0.90$, and $\Lambda = 1.3$ μm. Fig. 3 was calculated by using Ref. [41].

dispersion is greatly affected by the lattice pitch. The main reason is that the effect of material dispersion decreases, and the waveguide dispersion dominates. The X-polarization and Y-polarization fundamental mode operate in all-normal region when the fiber parameters are $\Lambda = 1.3$ μm, $d_1/\Lambda = 0.8$, and $d_2/\Lambda = 0.4$. To further increase the mode birefringence and reduce the confinement loss, we optimize the big (small) air hole air-filling fraction and set $\Lambda = 1.3$ μm.

In order to increase mode birefringence, meanwhile, reduce the confinement loss by changing the small hole diameter and fix the lattice pitch $\Lambda = 1.3$ μm. The mode birefringence increases as the air-filling fraction d_1/Λ increases, and varies slightly as the small air-hole changes [28]. The proposed LC-PCF works in all-normal dispersion region for the two polarized axis. The big hole air-filling fraction d_1/Λ varies from 0.8 to 0.9, nevertheless, the dispersion and confinement loss have changed slightly when fixed the value of d_2/Λ (Fig. 3(a) and (b)). The main reason is that the waveguide dispersion is slightly affected by big hole air-filling fraction as fixes the air hole pitch. And the smaller big air hole diameter makes the light confinement stronger. The fabrication of the optical fiber will become difficult when the big hole air-filling is more than 0.9. To obtain high birefringence and all-normal dispersion, we choose $d_1/\Lambda = 0.9$.

To further optimize the proposed fiber structure, we investigated the air-filling factor of small air holes d_2/Λ varies from 0.4 to 0.5. It is apparent that the chromatic dispersion has changed dramatically with an increase of the small air hole diameters (air-filling factor) (Fig. 3(c)), the main reason is that the small air hole diameter has great influence on waveguide dispersion as d_2/Λ changes from 0.4 to 0.5 at $d_1/\Lambda = 0.9$. The maximum GVD parameters are -47.3 ps·nm^{-1}km^{-1} (X-axis) and -8.5 ps·nm^{-1}km^{-1} (Y-axis) at wavelength $\lambda = 1.54$ μm and $\lambda = 1.46$ μm, respectively (Fig. 3(c)). The confinement loss decreases as increases d_2/Λ (Fig. 3(d)) due to tight mode confinement. In order to obtain high birefringence and make the proposed fiber operate in all-normal dispersion region, we select $d_2/\Lambda = 0.4$ as the air-filling factor of small air holes which is at expense of confinement loss. In order to obtain large spectral broadening, we select pump wavelength $\lambda = 1.55$ μm.

B. Supercontinuum Generation in Optimized Structure

The polarization evolution in our proposed highly birefringent PM-LCPCF is modeled with the two coupled generalized nonlinear Schrödinger equations (CGNLSE) as described in [45].

$$\frac{\partial A_j}{\partial z} + \frac{1}{2}\left(\Delta\beta_0 + \Delta\beta_1 \frac{\partial A_j}{\partial t}\right) - \sum_{m\geq 2} \frac{i^{m+1}}{m!}\beta_{mj}\frac{\partial^m A_j}{\partial t^m} = i\gamma\left(1 + i\tau_0\frac{\partial}{\partial t}\right) A_j \left[(1 - f_R)\left(|A_j|^2 + \frac{2}{3}|A_k|^2\right) + f_R \int_{-\infty}^{t} h_R(t - t')\left(|A_j|^2 + |A_k|^2\right) dt'\right] \quad (3)$$

where A_j and A_k are the field components with j and k = x or y (x≠y), z is a propagation coordinate, the time coordinate moving in a reference frame is given by $t = \tau$-$(\beta_{1j}+\beta_{1k})z/2$, $\Delta\beta_0 = (\beta_{0j}$-$\beta_{0k})$ is the phase mismatch, $\Delta\beta_1 = (\beta_{1j}$-$\beta_{1k})$ is the group velocity mismatch, τ_0 is optical shock time scale. The confinement losses are 0.09 dB·m^{-1} and 0.19 dB·m^{-1} (at pump wavelength of 1.55 μm) for X and Y polarized modes, respectively. Fiber loss is neglected because the short length of the fiber is considered in the simulations. All input pulses are assumed to be linearly polarized with no frequency chirp.

We show the dispersion coefficients (β) of the two orthogonal modes, the mode effective area A_{eff}, the nonlinear coefficient γ, and the birefringence B in Fig. 4. The first- and second-order dispersion terms of X-polarized mode and Y-polarized mode have different dispersion states due to fiber birefringence (Fig. 4(a)). The relationship between the first-order dispersion term and

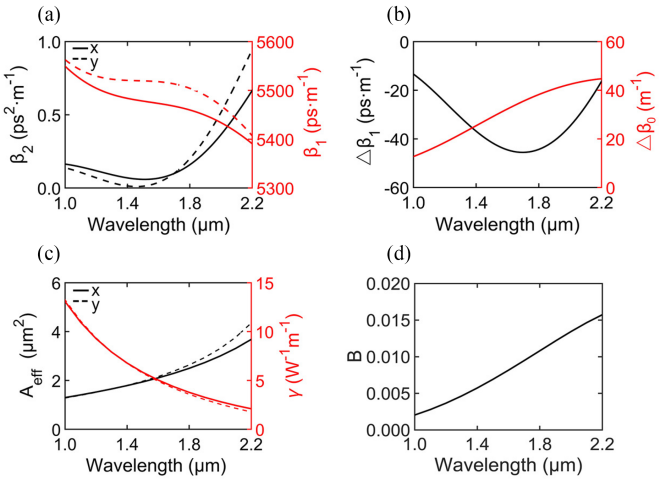

Fig. 4. The dispersion coefficients related to the mode propagation constant β, the mode effective area A_{eff}, the nonlinear coefficient γ and the birefringence B at $d_1/\Lambda = 0.9$, $d_2/\Lambda = 0.4$, and $\Lambda = 1.3$ μm. (a) The first- and second-order dispersion coefficients for the two fundamental modes, (b) The phase mismatch ($\Delta\beta_0$) and the group velocity mismatch ($\Delta\beta_1$) between the two fundamental modes. (c) The mode effective area A_{eff} and the nonlinear coefficient γ. (d) The mode birefringence B of the proposed LC-PCF versus wavelength. Fig. 4 was calculated by using Ref [46].

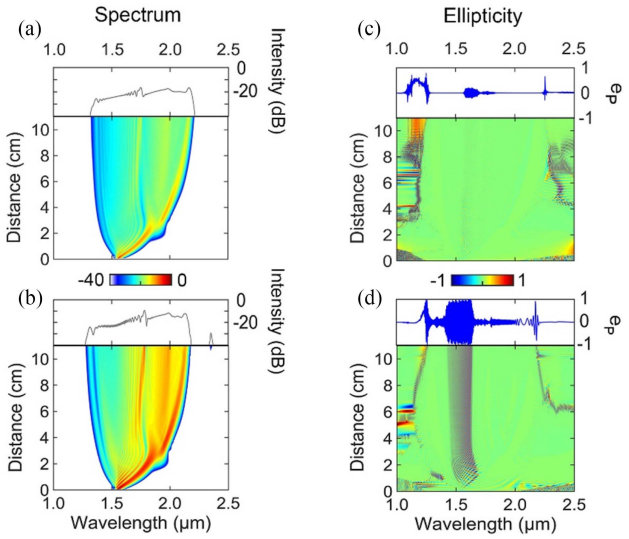

Fig. 5. Spectrum in log scale, ellipticity evolution with respect to propagating length along (a), (c) slow axis (0°) and (b), (d) fast axis (90°) of the proposed PM-LCPCF. The input pulse of $T_0 = 100$ fs has been launched at the peak power of 2 kW. Fig. 5 was calculated by using (1-4).

the group velocity is $\beta_1 = 1/v_g$. The group velocity mismatch reduces at first and then increases ($\Delta\beta_1 \leq -13.48$ ps·m-1) in the wavelength region of 1.0 μm to 2.2 μm (Fig. 4(b)). The minimum value of group velocity mismatch is $\Delta\beta_1 = -46.8$ ps·m^{-1} at $\lambda = 1.7$ μm. And the phase mismatch $\Delta\beta_0$ changes from 12.72 m^{-1} to 44.72 m^{-1} when the wavelength varies from 1.0 μm to 2.2 μm. The effective area A_{eff} increases and nonlinear parameter decreases when the wavelength changes from 1.0 μm to 2.2 μm (Fig. 4(c)). The mode area increases due to the mode field extending further into the cladding, and thus leads to smaller nonlinear coefficient with an increase in the wavelength. The effective area A_{eff} varies from 1.29 μm^2 to 3.67 μm^2 (X-axis) and from 1.28 μm^2 to 4.34 μm^2 (Y-axis), and the corresponding nonlinear parameter γ decrease from 13.1 W^{-1}·m^{-1} to 2.1 W^{-1}·m^{-1} (X-axis) and from 13.3 W^{-1}·m^{-1} to 1.77 W^{-1}·m^{-1} (Y-axis), respectively. The birefringence value increases from 2.04×10^{-3} to 1.57×10^{-2} as the wavelength varies from 1.0 μm to 2.2 μm (Fig. 4(d)). The main reason is that the mode field penetrates more into the asymmetrical cladding region as the wavelength increases.

The simulation method used in this study is the symmetrized split-step Fourier method utilizing a fourth order Runge Kutta method for the nonlinear integration. The response function and nonlinear parameters of carbon disulfide liquid are derived from Ref [47]. Random noise was added to our input condition and the results were sampled average 50 simulations. To characterize the polarization state and evaluate the pulse-to-pulse polarization fluctuations of the specific output SC, the parameter ellipticity e_p, and the polarization correlation function $\rho(\lambda)$ are generally used [48], respectively:

$$e_p = \frac{2\mathrm{Im}\left[\tilde{A}_x^*(\lambda)\tilde{A}_y(\lambda)\right]}{\left|\tilde{A}_x(\lambda)\right|^2 + \left|\tilde{A}_y(\lambda)\right|^2} \tag{4}$$

$$\rho(\lambda) = \frac{\left|\left\langle \tilde{A}_x(\lambda)\tilde{A}_y^*(\lambda)\right\rangle\right|}{\left[\left\langle\left|\tilde{A}_x(\lambda)\right|^2\right\rangle\left\langle\left|\tilde{A}_y(\lambda)\right|^2\right\rangle\right]^{1/2}} \tag{5}$$

where $\tilde{A}_x(\lambda)$ and $\tilde{A}_y(\lambda)$ are the Fourier transforms of $A_x(\tau)$ and $A_y(\tau)$, the angle brackets and the superscript '$*$' denote ensemble averaging and a complex conjugate operator, respectively. The ellipticity $e_p = 0$ represents that the output spectrum is linearly polarized light, and $e_p = \pm 1$ represent circularly polarized light. The maximum of polarization correlation denotes no fluctuations at all, and $\rho = 0$ indicates a totally random polarization state.

Modes on two orthogonal polarization axes are commonly considered as perfectly non-interacting modes, and there are almost no power coupling between two copropagating modes due to large group velocity mismatch which would prevent the energy transfer between both eigen-polarization modes when the pump peak power is low (such as $P_0 = 2$ kW) [41], [49]. We mainly discuss the influence of fiber length and pulse width on the output spectrum.

III. Numerical Results and Discussion

In the numerical simulation, the following parameters were used throughout this paper: a) the LC-PCF core-diameter 2R = 1.3 μm (at the pump wavelength of $\lambda_0 = 1.55$ μm; b) nonlinear refractive index $n_2 = 2.7 \times 10^{-18}$ m^{2}W^{-1} [50]; c) the hyperbolic secant pulse with duration $T_{FWHM} = 2\ln(1+\sqrt{2})T_0 \approx 1.763T_0$ (full width half maximum intensity); d) the pump power $P_0 = 2$ kW; e) the spectral bandwidth is determined -30 dB bandwidth; f) the fundamental mode birefringence B = 7.43×10^{-3}; g) the pulse polarization is aligned at angle $\theta = 0°$ to the slow axis (X-axis); h) we choose the dispersion coefficients up to the order of ten; g) the loss along the fiber length is no more

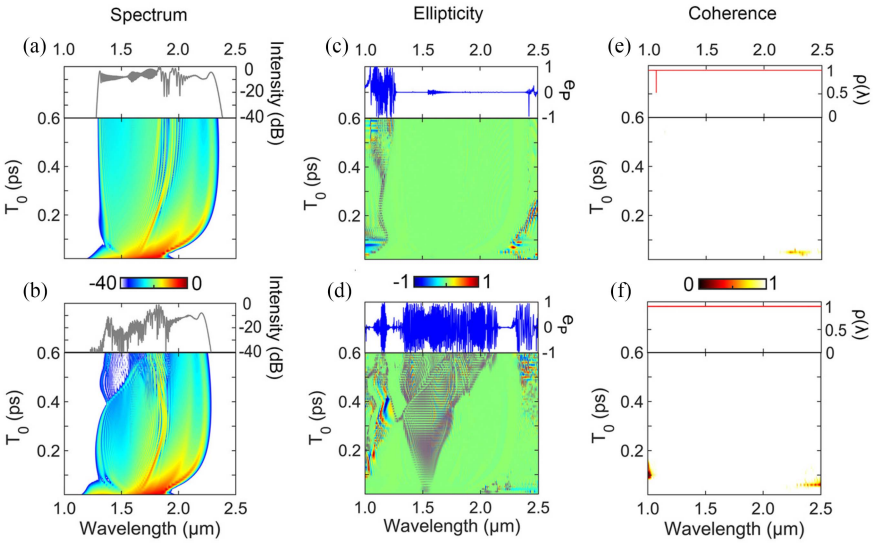

Fig. 6. Spectrum in log scale, ellipticity and coherence evolution with respect to pump pulse width along (a), (c), (e) slow axis (x-axis) and (b), (d), (f) fast axis (y-axis) of the proposed PM LC-PCF. The lattice pitch is $\Lambda = 1.3$ μm and the large (small) air hole fraction is $d_1/\Lambda = 0.9$ ($d_2/\Lambda = 0.4$). The input peak power of $P_0 = 2$ kW has been launched at the fiber length of $L = 7$ cm. Fig. 6 was calculated by using (1-5).

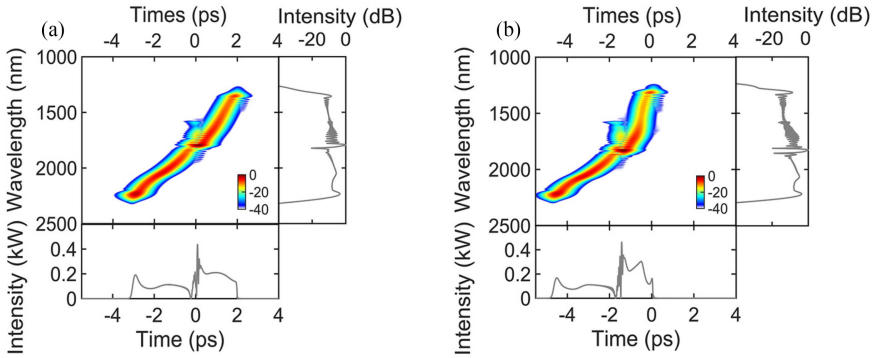

Fig. 7. Calculated XFROG trace with the structure of two orthogonal principal axis correlated with the intensity and spectrum showing evolution with propagation distance along (a) slow x-axis and (b) fast y-axis of the proposed PM-LCPCF. The input pulse of $T_0 = 200$ fs has been launched at the peak power of 2 kW for the length of L = 7 cm. Fig. 7 was calculated by using Ref. [46].

than 1 dB can be ignored; these can be considered as selection criteria of pump parameters or fiber parameter.

A. Influence of Fiber Length on Spectral width, Polarization of SC

Firstly, we study the influence of fiber length on the spectral profiles, ellipticity evolution when a pump pulse with center wavelength $\lambda_0 = 1.55$ μm, width $T_0 = 100$ fs, and peak power $P_0 = 2$ kW is launched into the slow (X-) axis ($\theta = 0°$) and fast (Y-) axis ($\theta = 90°$). Fig. 5(a) and (b) illustrate the SC broadening along the slow and fast axes for various lengths of the PM-LCPCF. In addition, as fiber length increases L from 0 cm to 11 cm, the bandwidth increases for X and Y polarized modes, respectively. The optical spectrum broadening is slightly when the fiber length is L> 7 cm in the X- and Y-polarized modes (Fig. 5(a) and (b)). The spectral broadening is dominated by self-phase modulation (SPM), and then the combination of GVD and self-phase modulation (SPM) make a strong-intensity pulse broaden. Those may result in optical wave breaking (OWB) induced by four wave mixing (FWM) when the pump was launched at slow (X)- or fast (Y)-axis in all-normal dispersion region. Due to quite short 100 fs pulse and short fiber length, the slow effect of simulated Raman scattering (SRS) does not occur in the presented case of SCG in the normal dispersion regime. The spectrum (-30 dB bandwidth) over the entire length is linear polarized light for ellipticity almost equal zero except for the region around the pump wavelength where the ellipticity is somewhat chaotic due to the presence of the undesired orthogonal pulse (Fig. 5(c)) for X polarized axes. For Y polarized mode the complicated wavelength dependence of the SC polarization state extends from both sides to the pump center wavelength when the fiber length is L>9 cm (Fig. 5(d)). And the polarization states show more sever changes around the pump wavelength for Y-polarized mode than X-polarized mode. The dramatic fashion results from the dominate SPM interaction with lower GVD (about 15 ps·nm^{-1}km^{-1}) for Y-polarized mode. So the fiber length be selected by $L<$ 9cm, and the optimum value

is $L = 7$ cm, at this point the bandwidth are broadened from 1355 nm to 2143 nm and from 1326 nm to 2116 nm for *X* and *Y* polarized axes, respectively.

B. Influence of Pulse Width on bandwidth, Polarization and Coherence of SC

Fig. 6 shows the influence of the pulse width on the SC bandwidth, polarization fluctuations and coherence with the input pump power of $P_0 = 2$ kW. The bandwidth (−30 dB) increases as pulse duration increases and starts to decrease after reaching a maximum value at a width of about $T_0 = 0.3$ ps and 0.24 ps for X and Y polarized axes, respectively, as the pulse duration increases from 0.05 ps to 0.6 ps (Fig. 6(a) and (b)). This is because the contribution of Raman response increases as the pulse duration increases. The pump pulse with large T_0 and small bandwidth will limit the process of spectral broadening in normal dispersion region. The spectrum expands from 1218−nm-1963 nm band to 1297 nm-2328 nm band and from 1179 nm-1943 nm band to 1808 nm-2241 nm band at pump wavelength of $\lambda_0 = 1.55$ μm when the pulse width varies from 0.05 ps to 0.6 ps, for X and Y polarized axes respectively. The spectrum (−30 dB bandwidth) over the entire pulse width (0.05 ps–0.6 ps) is about linear polarized light for the ellipticity being equal to zero except for the short wavelength region below 1.2 μm in the X polarized axes (Fig. 6(c) and (d)). The main reason is that the stimulated Raman scattering (SRS) was amplified as the pulse duration increase. But the severly chaotic ellipticity extends outwards from the region around the pump wavelength as the pulse width is $T_0 > 0.2$ ps in the Y polarized axes (Fig. 6(d)). This is because the smaller absolute dispersion peak value cause more severe splitting of spectrum. As was mentioned above, the absolute value of group velocity dispersion (GVD) of the proposed fiber are all-normal with 42 ps·nm^{-1}·km^{-1} and a peak of proximately 14 ps·nm^{-1}·km^{-1} at pump wavelength of $\lambda = 1.55$ μm in X and Y polarized axes, respectively. Therefore, the violent variation of polarization state results from the combination of the smaller group velocity dispersion (GVD) value, self-phase modulation (SPM) and stimulated Raman scattering (SRS) when the pulse width rises from 0.05 ps to 0.6 ps. The coherence is perfect because the polarization correlation degree is close to 1 (Fig. 6(e) and (f)). It indicates that Raman effect is insufficient to cause the amplification of quantum noise when the pulse duration is $T_0 \leq 0.60$ ps. Under comprehensive considering the wider and smoother SC spectra for two polarized axes, the pulse duration can be selected by $T_0 \leq 0.2$ ps. The optimum value of pulse duration is $T_0 = 0.2$ ps.

The shorter input pulse can help us obtain the smooth spectrum. So we selected the pulse duration of $T_0 = 200$ fs. Fig. 7 shows the numerically calculated the cross-correlation frequency-resolved optical gating(XFROG)trace, spectrum, and temporal waveform for the SC pulse of the two polarization axes at the propagation distance of $L = 7$ cm when the injected peak power is $P_0 = 2.0$ kW. The bandwidth are about 0.78 octave (1328 nm-2287 nm) and 0.81 octave (1281 nm-2245 nm) for X and Y polarized axes, respectively. Because the pump wavelength approaches to the maximum point of dispersion curve of X-axis, the spectral broadens more towards the long wavelength region in X-axis than in Y-axis (Fig. 7(a) and (b)). At such pump power ($P_0 = 2$ kW), the spectral broadening was primarily determined by self-phase modulation (SPM) and optical wave breaking (OWB) processes in normal dispersion region, then the spectrum was further broadened by the four-wave mixing (FWM) due to onset of OWB, thus the coherence of the pulse is kept to unity. The length of optical wave breaking ($L_{WB} = 1.1L_D/N$ derived from Ref [52]) are 8.6×10^{-4} m and 1.5×10^{-3} m. The oscillation of the spectrum near the pump wavelength in Fig. 7(a) is slighter than that in Fig. 7(b). The main reason is that large GVD corresponding to short light wave splitting length can reduce the depletion of the mid-section of the spectrum and be beneficial for smooth spectrum.

IV. Conclusion

We have numerically investigated the SC generation in core infiltration with CS_2 polarization maintaining photonic crystal fiber (PM LC-PCF). The proposed LC-PCF has an all-normal dispersion profile for the two orthogonal polarized axes, its mode birefringence reaches from 2.04×10^{-3} up to 1.57×10^{-2} in the wavelength range of 1 μm $\sim$ 2.2 μm. The polarization preserving highly coherent spectrum of SC has broadened from 1.32 μm to 2.28 μm and from 1.28 μm to 2.24 μm for X and Y polarized axes, respectively, when the pump power $P_0 = 2$ kW (0.35 nJ), the pulse duration $T_0 = 0.2$ ps and the LC-PCF length $L = 7$ cm are used at $\lambda = 1.55$ μm. In addition, we investigated the influence of pulse duration on the bandwidth, polarization state and coherence of the output spectrum. We have discovered that the linear polarization state of output light for X-axes is better than that of Y-axes as the pulse duration varies from 0.05 ps to 0.6 ps at the same pump wavelength. The proposed PM LC-PCF can be interestingly used in many fields such as biomedical imaging, frequency comb source, early cancer detection, food quality control, and sensing.

References

[1] J. M. Dudley and S. Coen, "Coherence properties of supercontinuum spectra generated in photonic crystal and tapered optical fibers," *Opt. Lett.,* vol. 27, no. 13, pp. 1180–1182, 2002.

[2] H. Ademgil, S. Haxha, T. Gorman, and F. AbdelMalek, "Bending effects on highly birefringent photonic crystal fibers with low chromatic dispersion and low confinement losses," *J. Lightw.. Technol.,* vol. 27, no. 5, pp. 559–567, Mar. 2009.

[3] X. Li, P. Liu, Z. Xu, and Z. Zhang, "Design of a pentagonal photonic crystal fiber with high birefringence and large flattened negative dispersion," *Appl. Opt.,* vol. 54, no. 24, pp. 7350–7357, 2015.

[4] D. Yoon Oh, K. Y. Yang, C. Fredrick, G. Ycas, S. A. Diddams, and K. J. Vahala, "Coherent ultra-violet to near-infrared generation in silica ridge waveguides," *Nature Commun.,* vol. 8, no. 1, pp. 1–7, 2017.

[5] F. Ganikhanov, S. Carrasco, X. Sunney Xie, M. Katz, W. Seitz, and D. Kopf, "Broadly tunable dual-wavelength light source for coherent anti-Stokes Raman scattering microscopy," *Opt. Lett.,* vol. 31, no. 9, pp. 1292–1294, 2006.

[6] Y. Geng, L. Wang, X. Tan, J. Wang, Y. Du, and X. Li, "A highly sensitive four-wave mixing-based microstructured fiber refractive index sensor for microfluid sensing applications," *Appl. Phys. Exp.,* vol. 12, no. 8, 2019, Art. no. 082008.

[7] I. Bargigia et al., "Time-resolved diffuse optical spectroscopy up to 1700 nm by means of a time-gated InGaAs/InP single-photon avalanche diode," *J. Appl. Spectrosc.,* vol. 66, no. 8, pp. 944–950, 2012.

[8] P. Del'Haye, A. Schliesser, O. Arcizet, T. Wilken, R. Holzwarth, and T. Kippenberg, "Optical frequency comb generation from a monolithic microresonator," *Nature,* vol. 450, no. 7173, pp. 1214–1217, 2007.

[9] T. Udem, R. Holzwarth, and T. W. Hänsch, "Optical frequency metrology," *Nature,* vol. 416, no. 6877, pp. 233–237, 2002.

[10] I. Hartl et al., "Ultrahigh-resolution optical coherence tomography using continuum generation in an air–silica microstructure optical fiber," *Opt. Lett.,* vol. 26, no. 9, pp. 608–610, 2001.

[11] H. Tu, D. L. Marks, Y. L. Koh, and S. A. Boppart, "Stabilization of continuum generation from normally dispersive nonlinear optical fibers for a tunable broad bandwidth source for optical coherence tomography," *Opt. lett.,* vol. 32, no. 14, pp. 2037–2039, 2007.

[12] P. Blandin et al., "Picosecond polarized supercontinuum generation controlled by intermodal four-wave mixing for fluorescence lifetime imaging microscopy," *Opt. Exp.,* vol. 16, no. 23, pp. 18844–18849, 2008.

[13] T. Hakala, J. Suomalainen, S. Kaasalainen, and Y. Chen, "Full waveform hyperspectral LiDAR for terrestrial laser scanning," *Opt. Exp.,* vol. 20, no. 7, pp. 7119–7127, 2012.

[14] Y. Tao and S. Chen, "All-fiber high-power linearly polarized supercontinuum generation from polarization-maintaining photonic crystal fibers," *High Power Laser Sci. Eng.,* vol. 7, pp. 1–6, 2019.

[15] V. V. Alexander et al., "Field trial of active remote sensing using a high-power short-wave infrared supercontinuum laser," *Appl. Opt.,* vol. 52, no. 27, pp. 6813–6823, 2013.

[16] B. Zhang, A. Jin, P. Ma, S. Chen, and J. Hou, "High-power near-infrared linearly-polarized supercontinuum generation in a polarization-maintaining Yb-doped fiber amplifier," *Opt. Exp.,* vol. 23, no. 22, pp. 28683–28690, 2015.

[17] Y. Liu et al., "Suppressing short-term polarization noise and related spectral decoherence in all-normal dispersion fiber supercontinuum generation," *J. Lightw. Technol.,* vol. 33, no. 9, pp. 1814–1820, May 2015.

[18] A. Rampur et al., "Ultra low-noise coherent supercontinuum amplification and compression below 100 fs in an all-fiber polarization-maintaining thulium fiber amplifier," *Opt. Exp.,* vol. 27, no. 24, pp. 35041–35051, 2019.

[19] N. Couture et al., "Polarization-resolved supercontinuum generated in a germania-doped photonic crystal fiber," *J. Phys. Photon.,* vol. 3, 2021, Art. no. 025002.

[20] E. Genier et al., "Ultra-flat, low-noise, and linearly polarized fiber supercontinuum source covering 670–1390 nm," *Opt. Lett,* vol. 46, no. 8, pp. 1820–1823, 2021.

[21] E. Genier et al., "Cross-phase modulation instability in PM ANDi fiber-based supercontinuum generation," *Opt. Lett.,* vol. 45, no. 13, pp. 3545–3548, 2020.

[22] A. LoredoTrejo, A. Díez, E. Silvestre, and M. V. Andrés, "Broadband tuning of polarization modulation instability in microstructured optical fibers," *Opt. Lett.,* vol. 45, no. 17, pp. 4891–4894, 2020.

[23] P. A. Agbemabiese and E. K. Akowuah, "Numerical analysis of photonic crystal fiber of ultra-high birefringence and high nonlinearity," *Sci. Rep.,* vol. 10, no. 1, 2020, Art. no. 21182.

[24] Y. Gao et al., "Highly-birefringent and ultra-wideband low-loss photonic crystal fiber with rhombic and elliptical holes," *Opt. Commun.,* vol. 450, pp. 172–175, 2019.

[25] S. Luke, S. K. Sudheer, and V. P. M. Pillai, "Modeling and analysis of a highly birefringent chalcogenide photonic crystal fiber," *Optik,* vol. 126, no. 23, pp. 3529–3532, 2015.

[26] M. Samiul Habib, K. M. Nasim, M. Selim Habib, M. Imran Hasan, and R. Ahmad, "Relative dispersion slope matched dispersion compensating highly birefringent spiral microstructure optical fibers using defected core," *Opt. Eng.,* vol. 52, no. 9, 2013, Art. no. 096110.

[27] Y. Yue et al., "Highly birefringent elliptical-hole photonic crystal fiber with squeezed hexagonal lattice," *Opt. Lett,* vol. 32, no. 5, pp. 469–471, 2007.

[28] T. Zhao, Z. Lian, T. Benson, X. Wang, W. Zhang, and S. Lou, "Highly-nonlinear polarization-maintaining As_2Se_3-based photonic quasi-crystal fiber for supercontinuum generation," *Opt. Mater.,* vol. 73, pp. 343–349, 2017.

[29] N. An, B. Zhuang, M. Li, Y. Lu, and Z.-G. Wang, "Combined theoretical and experimental study of refractive indices of water–acetonitrile–salt systems," *J. Phys. Chem. B,* vol. 119, no. 33, pp. 10701–10709, 2015.

[30] T. L. Canh et al., "Supercontinuum generation in all-normal dispersion suspended core fiber infiltrated with water," *Opt. Mater. Exp.,* vol. 10, no. 7, pp. 1733–1748, 2020.

[31] M. Chemnitz et al., "Carbon chloride-core fibers for soliton mediated supercontinuum generation," *Opt. Exp.,* vol. 26, no. 3, pp. 3221–3235, 2018.

[32] M. Chemnitz et al., "Hybrid soliton dynamics in liquid-core fibres," *Nature Commun.,* vol. 8, no. 1, pp. 1–12, 2017.

[33] M. Melnik, I. Vorontsova, S. Putilin, and A. Tcypkin, "The dependence of the supercontinuum coherence time in water jet on the input radiation intensity," *Appl. Phys. B,* vol. 126, no. 4, pp. 1–7, 2020.

[34] R. Zhang, J. Teipel, and H. Giessen, "Theoretical design of a liquid-core photonic crystal fiber for supercontinuum generation," *Opt. Exp.,* vol. 14, no. 15, pp. 6800–6812, 2006.

[35] D. Churin, T. N. Nguyen, K. Kieu, R. A. Norwood, and N. Peyghambarian, "Mid-IR supercontinuum generation in an integrated liquid-core optical fiber filled with CS_2," *Opt. Mater. Exp.,* vol. 3, no. 9, pp. 1358–1364, 2013.

[36] S. R. DS et al., "Ultra-low-noise supercontinuum generation with a flat near-zero normal dispersion fiber," *Opt. Lett.,* vol. 44, no. 9, pp. 2216–2219, 2019.

[37] A. M. Heidt, J. S. Feehan, J. H. Price, and T. Feurer, "Limits of coherent supercontinuum generation in normal dispersion fibers," *J. Opt. Soc. Amer. B,* vol. 34, no. 4, pp. 764–775, 2017.

[38] M. R. Karim, H. Ahmad, and B. M. A. Rahman, "All-normal-dispersion chalcogenide waveguides for ultraflat supercontinuum generation in the mid-infrared region," *IEEE J. Quantum Electron.,* vol. 53, no. 2, Apr. 2017, Art. no. 7100106.

[39] F. Xu et al., "Highly coherent supercontinuum generation in a polarization-maintaining CS_2-core photonic crystal fiber," *App. Opt.,* vol. 58, no. 6, pp. 1386–1392, 2019.

[40] Y. E. Monfared and S. A. Ponomarenko, "Extremely nonlinear carbon-disulfide-filled photonic crystal fiber with controllable dispersion," *Opt. Mater.*, vol. 88, pp. 406–411, 2019.

[41] M. Valliammai and S. Sivabalan, "Wide-band supercontinuum generation in mid-IR using polarization maintaining chalcogenide photonic quasi-crystal fiber," *Appl. Opt.,* vol. 56, no. 16, pp. 4797–4806, 2017.

[42] N. A. Mortensen, J. R. Folkenberg, M. D. Nielsen, and K. P. Hansen, "Modal cutoff and the V parameter in photonic crystal fibers," *Opt. Lett.,* vol. 28, no. 20, pp. 1879–1881, 2003.

[43] S. Kedenburg, T. Gissibl, T. Steinle, A. Steinmann, and H. Giessen, "Towards integration of a liquid-filled fiber capillary for supercontinuum generation in the 1.2–2.4 μm range," *Opt. Exp.,* vol. 23, no. 7, pp. 8281–8289, 2015.

[44] G. P. Agrawal, *Nonlinear Fiber Optics*, 4th ed. San Siego, CA, USA: Academic, 2010.

[45] I. Bravo Gonzalo, R. D. Engelsholm, M. P. Sørensen, and O. Bang, "Polarization noise places severe constraints on coherence of all-normal dispersion femtosecond supercontinuum generation," *Sci. Rep.,* vol. 8, no. 1, pp. 1–13, 2018.

[46] B. J. Chick, J. W. M. Chon, and M. Gu, "Polarization effects in a highly birefringent nonlinear photonic crystal fiber with two-zero dispersion wavelengths," *Opt. Exp.,* vol. 16, no. 24, pp. 20099–20105, 2008.

[47] C. Wang, G. Feng, W. Li, and S. Zhou, "Highly coherent supercontinuum generation in CS_2-infiltrated single-core optical fiber," *J. Opt.,* vol. 21, no. 10, 2019, Art. no. 105501.

[48] Z. Zhu and T. G. Brown, "Polarization properties of supercontinuum spectra generated in birefringent photonic crystal fibers," *J. Opt. Soc. Amer. B,* vol. 21, no. 2, pp. 249–257, 2004.

[49] E. R. Martins, D. H. Spadoti, M. A. Romero, and B.-H. V. Borges, "Theoretical analysis of supercontinuum generation in a highly birefringent D-shaped microstructured optical fiber," *Opt. Exp.,* vol. 15, no. 22, pp. 14335–14347, 2007.

[50] S. Kedenburg, A. Steinmann, R. Hegenbarth, T. Steinle, and H. Giessen, "Nonlinear refractive indices of nonlinear liquids: Wavelength dependence and influence of retarded response," *Appl. Phys. B,* vol. 117, no. 3, pp. 803–816, 2014.

[51] C. Finot, B. Kibler, L. Provost, and S. Wabnitz, "Beneficial impact of wave-breaking for coherent continuum formation in normally dispersive nonlinear fibers," *J. Opt. Soc. Amer. B,* vol. 25, no. 11, pp. 1938–1948, 2008.